02

Hydrogen defects in diamonds: research and definition of content of N3VH content using secondary ion mass spectrometry and infrared spectroscopy

© S.N. Shilobreeva¹, R.A. Khmelnitsky², B.Ya. Ber³, D.Yu. Kazantsev³, V.A. Dravin², V.Yu. Prokofiev⁴,S.A. Tarelkin⁵, M.V. Tokarev³

Moscow, Russia

Moscow, Russia

St. Petersburg, Russia

Moscow, Russia

e-mail: shilobre@mail.ru

Received January 27, 2025 Revised April 30, 2025 Accepted June 04, 2025

The concentration of hydrogen and N3VH defects in natural diamonds was determined using secondary ion mass spectrometry (SIMS) and infrared (IR) spectroscopy. A method for quantitative analysis of hydrogen was proposed based on the creation of reference samples directly in the studied samples by implantation of hydrogen. A linear correlation was established between the IR absorption of the paintwork material at 3107 cm⁻¹ and the hydrogen concentration determined by SIMS: $C_H = S_{N3VH}^* I_{3107}$, where $S_{N3VH}^* = (2.15 \pm 1.44) \cdot 10^{17}$ cm⁻¹. A detailed characteristics of main hydrogen defects in diamonds is given.

Keywords: IR spectroscopy, secondary ion mass spectrometry, diamond, hydrogen, N3VH defects.

DOI: 10.61011/EOS.2025.06.61661.7571-25

Introduction

Among all impurities in diamond, nitrogen holds first place in terms of significance and influence on its properties, while hydrogen ranks second. Studies of impurity composition show that the concentration of hydrogen in natural diamonds can reach up to 1% [1]. The so-called "hydrogen-rich" diamonds have been described [2-4]. This is not surprising given that natural diamond grows in an environment with high hydrogen content. Significant amounts of hydrogen and almost all oxygen are found within fluid inclusions inside diamond volumes as compounds such as H₂, CO₂, CH₄, H₂O, C₂H₄ and even C₂H₅OH [5,6]. These fluids may also surround solid-phase inclusions [7]. In Ref. [8] it was stated that perfect natural diamonds of gem quality type Ia without inclusions contain hydrogen at concentrations ranging from 500-3600 ppm, whereas low-nitrogen crystals of type IIa have lower levels up to 50 ppm [9,10] — which suggests a possible correlation between hydrogen and nitrogen impurities.

Hydrogen atoms directly decorate dislocations in the crystal structure of diamond, particularly edge-type dislocations where hydrogen atoms tend to saturate broken bonds [11,12]. In dislocations, C-H bonds exhibit dipole mo-

ments and should absorb infrared (IR) radiation, although so far hydrogen has not yet been identified in dislocations within diamond. Optically active hydrogen manifests itself through narrow lines primarily in the IR range [13]. Due to their small mass, atomic vibrational frequencies occur above 2700 cm⁻¹ which minimizes interference from other intrinsic absorption bands or defect-related complexes in diamond [2,14,15]. Natural diamonds display strong absorption lines at frequencies 2787, 3107, 3154, 3237, 4497 and $1405\,\mathrm{cm}^{-1}$, including one prominent line at $3107\,\mathrm{cm}^{-1}$ (line width 3 cm⁻¹) [3]. Synthetic diamonds and diamond films exhibit over a hundred distinct hydrogen LCM spanning $1384-6474 \,\mathrm{cm}^{-1}$ [16,17]. The highest-frequency lines often represent overtone combinations of valence and deformation vibration resonances of C-H and N-H bonds. Additionally, there exist absorption lines corresponding to transitions between excited electronic-vibrational energy levels In natural crystals with high hydrogen concentrations, many absorption lines and bands have been found in the visible and near IR regions [2-4]. The large number of LCM reflects (but not exhaustively) the wide variety of hydrogen forms in synthetic and natural diamonds. However, over time, it became clear that in natural and synthetic diamonds, a

 $^{^{\}rm 1}\,\text{V.I.}$ Vernadsky Institute of Geochemistry and Analytical Chemistry,

² Lebedev Physical Institute, Russian Academy of Sciences,

³ loffe Institute,

⁴ Institute of Geology of Ore Deposits, Petrography, Mineralogy, and Geochemistry of RAS,

⁵ Technological Institute for Superhard and Novel Carbon Materials National Research Center "Kurchatov Institute", Troitsk. Russia

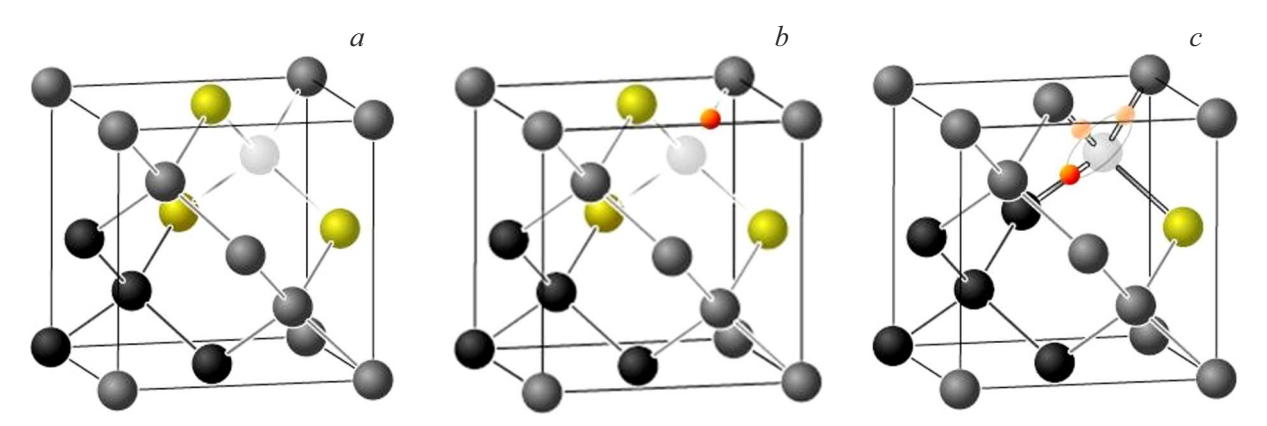


Figure 1. Atomic structures of defects N_3V , N_3VH^0 and NVH-. Carbon atoms are shown in gray, nitrogen atoms — yellow, hydrogen atoms — red, carbon vacancy — light gray. (a) Structure of the N_3V defect, (b) structure of the N_3VH defect, (c) structure of the defect NVH^- . The hydrogen atom moves between bonds with three adjacent carbon atoms.

significant portion of hydrogen may be in an optically inactive state [11,18].

A wide variety of point defects in both synthetic and natural diamond lattices involve hydrogen, nitrogen, and vacancies (V). Major sets of point defects in diamond include [19]: N, N₂, V, NV, N₂V, N₃V, N₄V, N₄V₂, VH, NVH, N₂VH, N₃VH, VH₂, NVH₂, N₂VH₂, VH₃, NVH₃, VH₄. These defects appear in different charge states, leading to centers detectable via electron paramagnetic resonance (EPR), optical absorption, and IR spectroscopy. However, none of these EPR centers in natural diamonds [20] contains hydrogen. The N₄VH configuration is energetically unfavorable and is not found in diamonds. When growing a diamond enriched with the ¹⁵N isotope, it turned out that the IR absorption frequencies of defects of the N_nVH (n = 1 - 3) series do not change. Taking into account also the data of measurements in synthetic crystals with an increased content of the ¹³C, isotope, it can be assumed that the hydrogen atom in all these defects is located on C-H [19,21] bond.

One particular defect stands out — the N₃VH. Its structure was established in studies [22,23] (Fig. 1, a), especially through analyses involving isotopes of carbon, nitrogen, and hydrogen. [24]. Being in a neutral-charge-state, it absorbs IR radiation at 3107 cm⁻¹ (stretch vibrations mode) and 1405 cm⁻¹ (deformation vibrations mode). It represents the final stable member of the sequence VH, NVH, N2VH, N₃VH making it a product of high-temperature annealing in synthetic diamonds [25] and long-term natural diamond annealing. On the other hand, N₃VH resembles another well-known defect — N₃V (Fig. 1, a), responsible for the important optical center N3 with zero-phonon-line (ZPL) emission at 415 nm. Together with its vibronic replica N2 emitting at 478 nm, this contributes significantly to yellow hues characteristic of Type-Ia natural diamonds known as "Cape Yellow". In addition, the optical center N3 gives very bright luminescence with a ZPL of 415 nm and is found in all natural diamonds without exception, even in

low-nitrogen type IIa diamonds. Moreover, it does not appear in IR due to its negligible concentration [10]. In the N₃V defect, one carbon atom has an unsaturated bond. When the unsaturated bond in N₃VH [19,25] is saturated by a hydrogen atom, it forms, resulting in fully completed bonds (Figure 1, b). It has a symmetry $C_{3\nu}$, exhibits no electrical charge, cannot act as an acceptor, lacks energy levels within the bandgap, and possesses zero spin. Consequently, it does not demonstrate any optical absorption, luminescence, or activity in EPR. Thus, the defects N₃V and N₃VH are related and in natural crystals (subjected to prolonged annealing in the depths of the Earth at temperatures of 1000-1300 °C) they represent stable configurations of nitrogen-vacancy and nitrogen-vacancyhydrogen defects, respectively. The N₃VH defect (Fig. 1, b) is formed during annealing above 2100 °C in synthetic HPHT crystals CVD [10]. It has been established that the concentration of N₃VH defects in natural diamonds is limited by the concentration of the main nitrogen defects of types A and B [25]. In CVD crystals grown in a hydrogen atmosphere, given the small size of the hydrogen atom and its high mobility, a high content of impurity hydrogen should be expected. Determined by nuclear-physical methods, it reaches tenths of a percent, but dislocations are declared to be the main location of impurity hydrogen [26]. nitrogen-containing irradiated and annealed CVD crystals, the formation of NVH defects is observed, which in the neutral charge state give a narrow line in the IR spectrum at 3123 cm⁻¹ [27]. As a result of annealing, vacancies and hydrogen atoms bind to single nitrogen atoms, forming an NVH defect, the atomic structure of which is shown in Fig. 1, c. However, it is not clear in what form hydrogen was in the crystal lattice of CVD crystals before annealing.

In CVD crystals with NVH defects, there are also always dominant in concentration single nitrogen atoms in the substitutional position — these are type C defects. In such a position in the diamond crystal lattice, nitrogen is

a deep donor — its activation energy is 1.7 eV. When such a crystal is illuminated with light with a higher quantum energy or as a result of high-temperature annealing, donor nitrogen gives up an electron to the conduction band. Such electrons are effectively captured by the NVH defect, transferring it to the negative charge state NVH⁻. The NVH⁻ defect in the ground state has a spin of 1/2 and at temperatures above $10 \, \text{K}$ is identified as an EPR center with an unexpected symmetry C_{3v} [28], which is explained by the rapid movement of a hydrogen atom between three carbon atoms (Fig. 1, c).

The EPR method can be used to measure the absolute number of paramagnetic centers (in this case, equal to the content of NVH⁻defects) in a crystal. In illuminated or annealed synthetic diamonds, due to an increase in the concentration of NVH⁻ defects, the EPR signal increases, and the absorption of the 3123 cm⁻¹ line (the concentration of NVH⁰ defects) decreases. Comparison of simultaneous and oppositely directed changes in the intensity of lines in the IR spectrum and EPR signals made it possible to obtain a calibration dependence of the concentration of NVH⁰ S_{NVH} 3123 cm⁻¹ [29]:

$$C_{\text{NVH}}^0 = S_{\text{NVH}} I_{3123}. \tag{1}$$

Here $C_{\rm NVH}^0$ is the concentration of 0 defects (in ppb units), I_{3123} — is the area under the absorption line 3123 cm⁻¹ (in cm⁻² units). At room temperature and a low concentration of NVH⁰ defects, the 3123 cm⁻¹ line (as well as other paint and varnish lines) has a Lorentzian shape at half-maximum (FWHM) of approximately 3 cm^{-1} . In the 2009-2010dissertations of Ph.D. candidates from the University of Warwick [23,30] the value $S_{\text{NVH}} = (330 \pm 30) \text{ ppb cm}^2$ is However, in the 2014 dissertation of the same school [28] (with a reference to the dissertation [23]) a different calibration is given: $S_{\text{NVH}} = (200 \pm 15) \text{ ppb cm}^2$. The same calibration is given in the 2020 work of employees of the same research group [31]. In the paper [28] it is stated that the calibration coefficients for the N_3VH^0 (S_{N_3VH}) defect and the NVH 0 (S_{NVH}) defect should be close. The rationale for this is that the C-H bonds and atomic environments in these defects are similar, and the oscillation frequencies differ little. However, in our opinion, there are differences: in the NVH defect, the hydrogen atom quickly moves between three carbon atoms and, unlike the N₃VH defect, the deformation mode of its oscillations does not manifest itself.

Until recently, direct calibration for estimating the concentration of N_3VH defects by IR absorption was absent. In the fundamental work [31] the spectral and temporal characteristics of this defect were studied by the pump-probe method on three diamonds (one CVD, two natural), due to which a picture of its electron-vibrational structure and excitation relaxation mechanisms was constructed. In particular, in addition to the electron-vibrational transition from the ground (principal quantum number n=0) to the first excited level (n=1) with

a frequency of 3107 cm⁻¹ a transition from the first excited (n = 1) to the second excited level (n = 2) with a frequency of 2963 cm⁻¹ was revealed. The decrease in the frequency is due to the nonlinearity of the dependence of the potential energy of the V(r) defect on the r coordinate (in this case r is the C-H bond length). To describe the transition in works [31,32] a simple two-parameter Morse potential (Morse) adopted in molecular spectroscopy was used: $V(r) = D_e(1 - e^{-a(r-re)})^2$. It allows one to calculate the energies of the ground and excited (1, 2, etc.) states during vibrations relative to the equilibrium position r_e . The values of the transition frequencies of 3107 and 2963 cm⁻¹ allowed one to determine the parameters of the model Morse potential N₃VH of the defect: $D_e = 4.56 \,\mathrm{eV}$ and $a = 2 \cdot 10^8 \,\mathrm{cm}^{-1}$ [31]. The Morse potential is convenient in that it makes it possible to explicitly calculate the matrix element of the transition during the absorption of electromagnetic radiation, in particular, for the 3107 cm⁻¹ line, and therefore calculate the optical absorption crosssection and, consequently, obtain a concentration calibration for N₃VH defects based on the absorption of IR radiation. In works [31,32] the value of the calibration coefficient $S_{\rm N3VH} = (110 \pm 10) \, \rm ppb \, cm^2 = (1.94 \pm 0.18) \cdot 10^{16} \, cm^{-1}$ is given, which is two times less than the value of $S_{\rm NVH}$ obtained in the same works. Note that $S_{\rm N3VH} = (110 \pm 10) \, \rm ppb \, cm^2$ is a small value, in other words, a very real concentration of N₃VH defects $C_{\rm N3VH} \sim 100 \, \rm ppm$ corresponds to an absorption of IR radiation $I_{3123} \sim 1000 \, \mathrm{cm}^{-2}$, which is not observed in practice.

Thus, the N₃VH complex is the main observed hydrogencontaining defect in perfect natural diamonds. The aim of this work is to experimentally study the ratio of the N₃VH defect concentration based on IR absorption measurements in 3107 cm⁻¹ LCM in comparison with the hydrogen concentration determined by secondary ion mass spectrometry (SIMS). In general, the work follows the approach described earlier [32,33] and methodologically complements it.

Experiment Using IR Spectroscopy

We used thin polished plane-parallel wafers cut from natural diamonds, oriented close to (110) with thickness ranging from 150– to 650 μ m), and linear dimensions of 3–5 mm. Natural diamonds were used because the set of hydrogen defects in them is much narrower than in synthetic ones due to long-term annealing at average temperatures in the Earth's interior, and the N₃VH defect is the final member of the nitrogen-hydrogen defect aggregation sequence [34]. HPHT synthetic diamonds are characterized by a highly heterogeneous distribution of impurities and defects throughout the volume (especially in different growth sectors). And CVD crystals are characterized by a very high dislocation density (typically $10^6 - 10^8$ cm⁻²), which can contain a lot of hydrogen. In the first stage, IR absorption in the range of 400-4000 cm⁻¹ with circular diaphragms

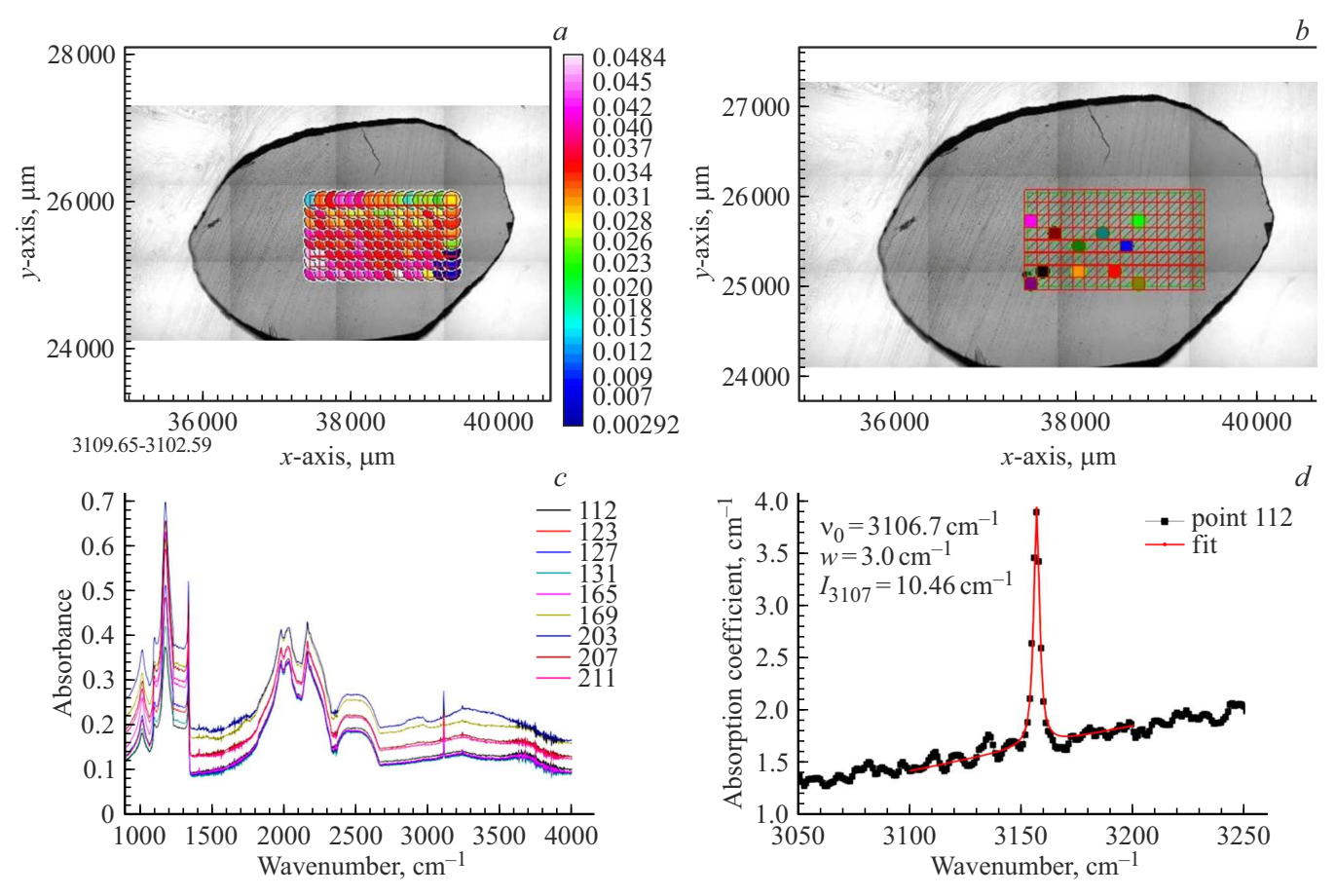


Figure 2. (a) View of one of the plates (T219) indicating the region of uniform IR absorption distribution selected at the second stage of IR measurements (the color shows the integrated optical absorption on the line $3107 \, \mathrm{cm}^{-1}$ minus the baseline in the range $3050-3150 \, \mathrm{cm}^{-1}$); (b) measurement locations with a high signal-to-noise ratio at the third stage of IR measurements (individual measurement locations are marked with different colors); (c) IR absorption spectra at the measurement locations selected at the third stage indicating the measurement point numbers; (d) Lorentzian representation of the LCM $3107 \, \mathrm{cm}^{-1}$, the error in determining the absorption coefficient is $0.1 \, \mathrm{cm}^{-1}$.

of 2 and 1 mm diameters was measured at different places on the plates using a Bruker70v spectrometer. This allowed us to preliminarily estimate the average absorption on the $3107 \, \mathrm{cm}^{-1}$ line. Of the 27 studied wafers, 6 samples were selected that met the following criteria.

- 1. Contain only N_3VH defects (LCM 3107 and $1405\,\text{cm}^{-1}$) according to IR spectroscopy.
- 2. The amplitude of the line at $3107\,\mathrm{cm^{-1}}$ does not exceed the intensity of the intrinsic two-phonon absorption in the range of $1400-2660\,\mathrm{cm^{-1}}$ (< $12\,\mathrm{cm^{-1}}$). This excludes the so-called "hydrogen-rich" crystals from the study.
- 3. No mineral or fluid inclusions are detected in the wafers when viewed in transmission through an optical microscope, and the dislocation density according to the results of birefringence analysis does not exceed 10⁴ cm⁻²;
- 4. The spread of the line intensity at 3107 cm⁻¹ in different places of the sample when measured with an aperture of 1 mm does not exceed two times. As shown in [35], the distribution of the main defects (including

theN₃VH) defect) over the volume of natural crystals can be very non-uniform;

5. IR absorption measurements are performed in transmission through the entire sample, and SIMS measurements affect only the near-surface layer with a thickness of no more than $10\,\mu\text{m}$. There is no guarantee that the concentrations of the studied defects near the surface and in the depth of the sample are the same. To minimize this discrepancy, the thinnest possible plates should be used.

In the table, the samples selected for study are described. Subsequent infrared absorption measurements were carried out on a scanning IR Fourier microscope LUMOS (Bruker) in the range of $1000-4000\,\mathrm{cm^{-1}}$. A square measuring diaphragm $120\times120\,\mu\mathrm{m}$ was used. This diaphragm was utilized at the second stage of IR measurements over the entire surface of each sample in sequential 2D scanning to perform fast (1 scan) IR absorption measurements (in the range of $800-4000\,\mathrm{cm^{-1}}$) to select the places with the most uniform I_{3107} distribution. A part of such a map for one of the samples in the form of a rectangular area is shown in

Number of the sample	Orientation	Polishing	Thickness, μm	Integral coefficient LCM absorption 3107 cm ⁻¹ , cm ⁻²	Type by content of nitrogen
T210	(110)	Polished	401 ± 5	3.5 ± 0.9	IIa-IaB
T216	(110)	Polished	414 ± 9	$14,7 \pm 3.8$	IaB
T219	(110)	Polished	112 ± 25 , wedge-shaped	13.3 ± 3.0	IaB
T221	(100)	Polished	219 ± 6	15.3 ± 2.7	IaB
T284	(111)	Unpolished, by the flat chipping area	625 ± 17	1.7 ± 0.5	IaAB
T286	(110)	Polished	260 ± 10	2.9 ± 0.9	IIa

Characteristics of the studied diamonds

Note: The notation is as follows: IIa — low-nitrogen diamond without one-phonon IR absorption; IaB — one-phonon absorption $(400-1400\,\mathrm{cm}^{-1})$ on nitrogen defects (in this case B-defects (N_4V)) is greater than the intrinsic two-phonon absorption $(1400-2700\,\mathrm{cm}^{-1})$; IIa-IaB — less; IaAB — contains defects A and B.

Fig. 2, a. To the right of the map is the scale of the optical absorption integral I_{3107} in LCM 3107 cm⁻¹ after removing the baseline. From Fig. 2, a it is evident that the region of the sample with the most uniform I_{3107} distribution is located in the lower left part of the rectangular area. At the third stage of measurements, it was in this area that the measurement points of the IR absorption spectra with a high signal-to-noise ratio were selected (10 scans each). These points are marked with different colors in Fig. 2, b, shows the IR spectra measured at these points, Fig. 2, d — one of the spectra in the vicinity of the LCM $3107 \,\mathrm{cm}^{-1}$. The infrared absorption spectra were processed by numerical approximation of the IR absorption peak at 3107 cm⁻¹ using the least squares method. For the approximation, the sum of the linear function of the background absorption and the Lorentz function was used:

$$\alpha(\nu) = \alpha_0 + k\nu + \frac{2I_{3107}w}{\pi(4(\nu - \nu_0)^2 + w^2)},$$
 (2)

where ν — wavenumber, cm⁻¹; $\alpha(\nu)$ — optical absorption, cm⁻¹; α_0 and k — parameters of the linear function of background approximation; ν_0 — position of the peak maximum along the wavenumber axis, cm⁻¹; I_{3107} — integrated intensity of the Lorentzian peak, cm⁻²; w is the full width at half maximum (FWHM) of the Lorentzian peak, cm⁻¹. Approximation was conducted in the wavenumber interval between 3050 and 3150 cm⁻¹. The amplitude of the Lorentzian peak (cm⁻¹) can be calculated from the approximation parameters according to the formula: $A_{3107} = 2I_{3107}/\pi w$.

Experiment Using SIMS Technique

For areas of the samples characterized by maximally uniform distribution of I_{3107} SIMS measurements were then executed at the fourth stage. At least five depth

profiles of hydrogen concentration per side of each wafer (totaling no fewer than ten per platelet) were obtained in the regions designated during the third-stage IR measurements. The SIMS profiling technique involves focused primary ion beams sequentially removing layers of the target material while simultaneously mass-spectrometrically analyzing the elemental composition of secondary ions emitted from the bottom of the ion etching crater upon sputtering the target. This process registers intensities of various types of ions (positive or negative, monoatomic or polyatomic) depending on the time elapsed since ion etching began. Such data allows us not only to convert ion etching times into current depths of the position of the etching crater bottom, from which the ions were emitted at the given moment, but also, using the necessary calibrations, to determine the concentration (content) of impurities at the given moment of etching time (i.e. at the given depth) based on the set of current intensities of secondary (analytical) ions. Collectively, datasets of the form *impurity* concentration versus depth of ion etching represent a SIMSprofile illustrating impurity distributions through uniformly (matrix) composed targets [36].

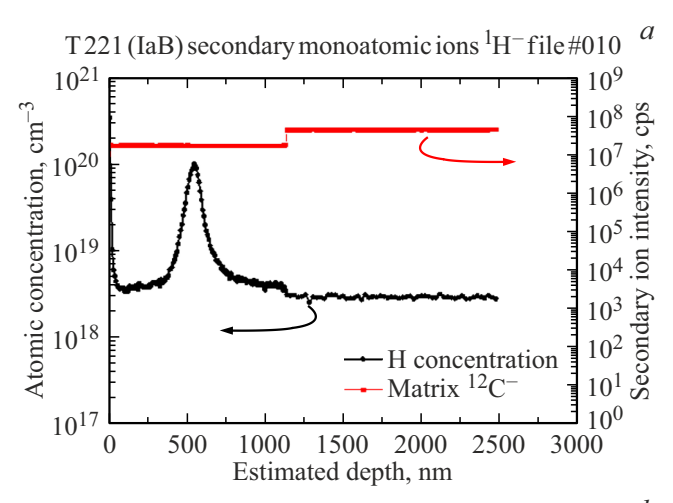
Typically, calibration standards for quantitative SIMS analysis of impurities involve external reference samples either devoid of or containing minimal amounts of the analyte impurity, into which known quantities of that impurity have been introduced via ion implantation [32,33]. With this approach, the found calibration values (relative sensitivity factors, RSF) can be used in the analysis of the studied samples only if all the fine adjustments of the primary and secondary ion optics of the SIMS instrument, the geometry of the target location in the analytical chamber and other parameters accurately reproduce the conditions under which the RSF was previously determined, making it labor-intensive and sometimes incomplete. To address this challenge, prior to SIMS profiling in our work, we

implanted ¹H⁺ ions in every studied sample, both sides receiving doses of 10^{15} cm⁻² at energy levels of 100 keV. To carry out ion implantation, an ion implanter from High Voltage Engineering Europe B.V. (Netherlands) was used. This resulted in bell-shaped hydrogen concentration distributions beneath the diamond surfaces with characteristic depths (projective range of ions in the target R_p) around 500 nm and well-known total numbers of atoms involved (Fig. 3). Hydrogen concentrations beyond $2-3R_p$, where the diamond structure remains essentially undistorted by ion implantation processes and radiationstimulated diffusion at room temperature [37,38] correspond to native hydrogen content in the diamond requiring determination.

During measurements, pressure in the SIMS instrument's analytical chamber reached values up to $2\cdot 10^{-10}\,\text{Torr.}$ Despite these conditions, investigations into solid-state targets' contents of "volatile" elements like hydrogen, carbon, oxygen, and nitrogen face complications due to their incorporation into molecules constituting residual atmospheric gases present even under ultra-high vacuum conditions in the SIMS tool's analytical chamber. Consequently, these elements continuously adsorb onto the investigated sample's surface before being ejected as ions following ion etching. Thus, the observed current of analytical ions arises partly from atoms contained within the sample itself — the object of investigation — and partly from analogous atoms originating from residual gas components within the tool's atmosphere. The first component scales linearly with the rate of ion etching, i.e., the density of the primary ion beam. The second component does not depend on etching rate. Therefore, minimizing the relative contribution of the latter term necessitates increasing the ion etching speed until technical limitations of the equipment are met. In this study an increase in the primary beam current density was achieved by reducing the raster size. Etching speeds consequently rose several-fold towards the final stages of SIMS profiling, transitioning from initial rasters [39] sized $70 \times 70 \,\mu\text{m}$, down to final rasters reduced to smaller dimensions $30 \times 30 \,\mu\text{m}$, hereby significantly enhancing etching speeds.

At least five hydrogen concentration profile measurements across the depth dimension were conducted per side of each sample (thus at least ten per wafer) throughout the SIMS profiling process. Measurement locations corresponded to those previously identified in Stage Three IR analyses.

To prevent contamination prior to measurements, samples underwent degreasing in boiling ethanol. Due to the necessity of investigating samples from both sides, they were fixed onto carriers using specialized ultrahigh-vacuum adhesive tape. Since diamond is an insulator whose surface charges when bombarded by primary ions, rendering SIMS measurements impossible. Steps were taken to suppress charging effects. Specifically, a thin layer of gold $\sim 20\,\mathrm{nm}$ thick, was pre-deposited onto the sample surface, followed by continuous irradiation with slow electrons during the



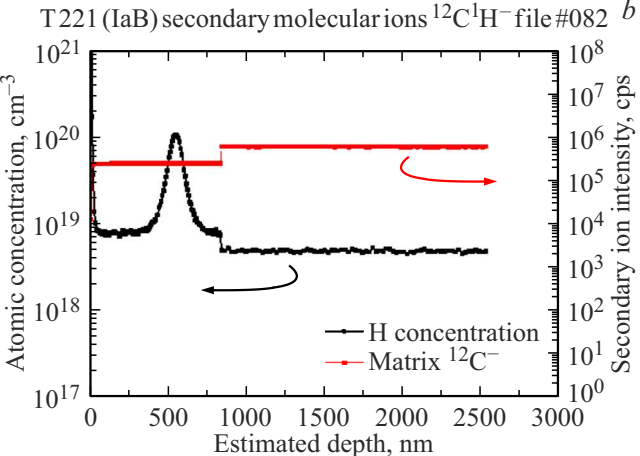


Figure 3. SIMS Profile of Depth Distribution of Hydrogen Impurity in Diamond Ion-Implanted with $^{1}H^{+}$ (dose $1 \cdot 10^{15}$ cm $^{-2}$, energy 100 keV). See text for details.

measurement process. These measures ensured maintenance of the sample's surface potential at 0 V. during the experiment.

For SIMS measurements, we utilized a CAMECA IMS-7F (France) secondary ion microprobe instrument combining magnetic-sector mass spectrometry with double focusing capabilities. Primary $^{133}\mathrm{Cs^+}$ ions with kinetic impact energies of 15 keV, were used for ion sputtering. Initially, the focused beam scanned the sample surface in rasters of size $70\times70\,\mu\mathrm{m}$ during profiling of implanted hydrogen atoms (down to depths exceeding $1000\,\mu\mathrm{m}$), subsequently shrinking to a raster size of $30\times30\,\mu\mathrm{m}$, i.e., at an increased ion sputtering rate, at the stage of profiling the hydrogen content in the sample.

Analytical secondary ions consisted of pairs *ion containing impurity atom* — *ion containing matrix atom* in forms such as $^{1}H^{-}-^{12}C^{-}$ or $^{1}H^{12}C^{-}-^{13}C^{-}$. The depth scale of the SIMS profile was determined from data on the time dependence of secondary ion currents by measuring the depth of the diamond etching crater using a primary ion raster of size $70 \times 70 \,\mu m$ using an AMBiOS XP-1 (USA)

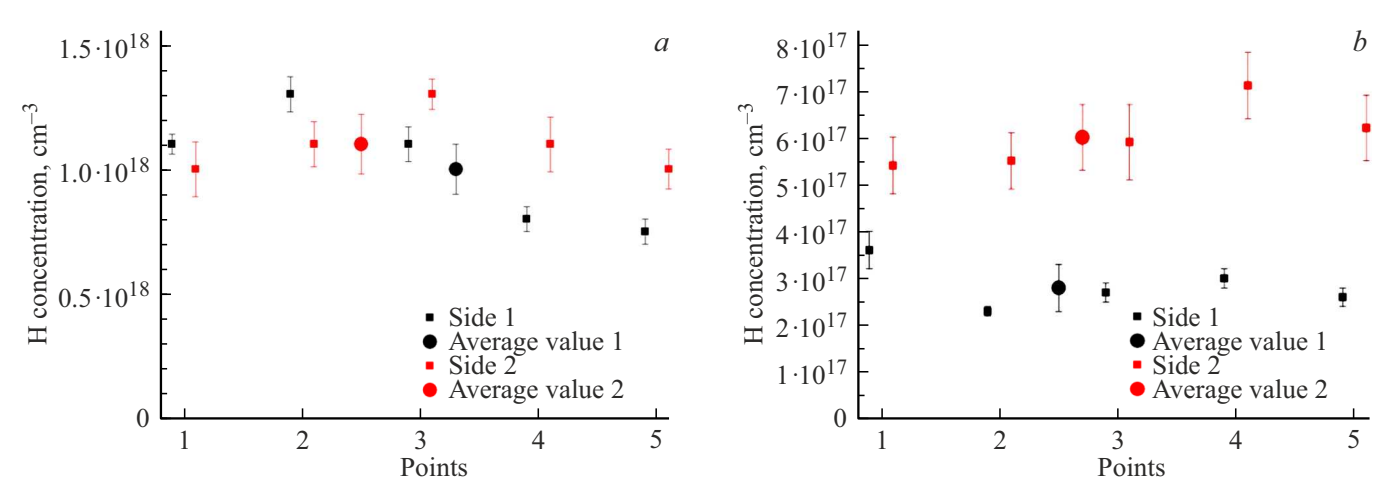


Figure 4. The results of calculating hydrogen concentrations based on the SIMS measurements at different points in the selected measurement areas and on two sides of the plates: (a) a sample with similar hydrogen concentrations on two sides (T210), (b) a sample with very different hydrogen concentrations on two sides (T284).

profilometer and from data for profile sections measured with a smaller raster size. The depth was estimated taking into account the increase in the primary beam current density and, accordingly, the increase in the ion etching rate.

The hydrogen impurity content was determined using the standard procedure for determining the RSF for ion-implanted samples [40,41] on a section of the profile representing a bell-shaped curve, using the dose of implanted hydrogen assigned to them (dose $10^{15}\,\mathrm{cm}^{-2}$). The RSF value determined in this way was used to calculate the depth distribution profile of the hydrogen impurity in the diamond for the entire profile, including its final part, the hydrogen concentration in which was taken as an estimate of the upper limit of the hydrogen content in this region of the diamond sample.

During the measurements, it turned out that a significant (at least 50%) share of the profiles had an anomalous and irregular appearance. It is possible that in these cases, hydrogen-containing microscopic inclusions (most likely fluid) were encountered during ion profiling, which were also found in [33]. These inclusions are so small that they are invisible under a microscope and the IR absorption signal from the substances they contain is below the sensitivity of IR spectroscopy [35]. However, if foreign inclusions were the cause, the irregularities should have been observed at different depths, but we observed them mainly in the near-surface layer. There is another explanation. In [40] it was found that in some places the near-surface layer of diamond contains some unknown extended defects through which implanted atoms can diffuse to the surface. The results of SIMS profiling demonstrating such anomalous profiles were excluded from consideration and a new SIMS profiling was performed on an adjacent area of the sample demonstrating the expected impurity distribution in the form of a signal from a bell-shaped profile of implanted hydrogen

superimposed on a constant signal from hydrogen located in the diamond and hydrogen originating from the gases of the analytical chamber adsorbed on the surface of the sample. A typical profile of the hydrogen content in the samples is shown in Fig. 3. The breaks in the profiles at depths greater than 1000 nm correspond to the moment of change in the primary beam raster size from $70 \times 70\,\mu\mathrm{m}$ to $30 \times 30\,\mu\mathrm{m}$ after which the ion etching rate and, consequently, the current of secondary ions of carbon isotopes increase several times. Fig. 4 shows, as an example, the results of calculating the concentrations of impurity hydrogen on two sides of the plates for two samples — on each side there are five points of the SIMS analysis. The average values of hydrogen concentrations over all measurements are also given.

Among the six studied samples, on one of them (with the greatest thickness T284), according to the SIMS data, the different sides of the wafer differed greatly in hydrogen concentration values (Fig. 4, b). This sample was excluded from consideration. For the remaining five samples (Fig. 4, a), within the measurement error, as well as within the statistical spread, the hydrogen concentration values on two sides of the wafers and at different points in the selected analysis areas turned out to be suitable for statistical analysis. If the impurity concentrations on both sides of a thin wafer are close, then there is reason to consider its concentration to be approximately constant over the entire thickness of the wafer in the measurement area.

As can be seen in Fig. 4, the hydrogen concentration values determined by the SIMS method in different places of the selected analysis area may differ by tens of percent. In order to increase the representativeness and accuracy of the data, at the fifth stage of the study, the absorption of IR radiation was measured at the locations of craters from SIMS profiling using a Bruker70v spectrometer with an $200 \times 200 \, \mu \mathrm{m}$ diaphragm. Thus, at least 10 measurements were made for each of the samples.

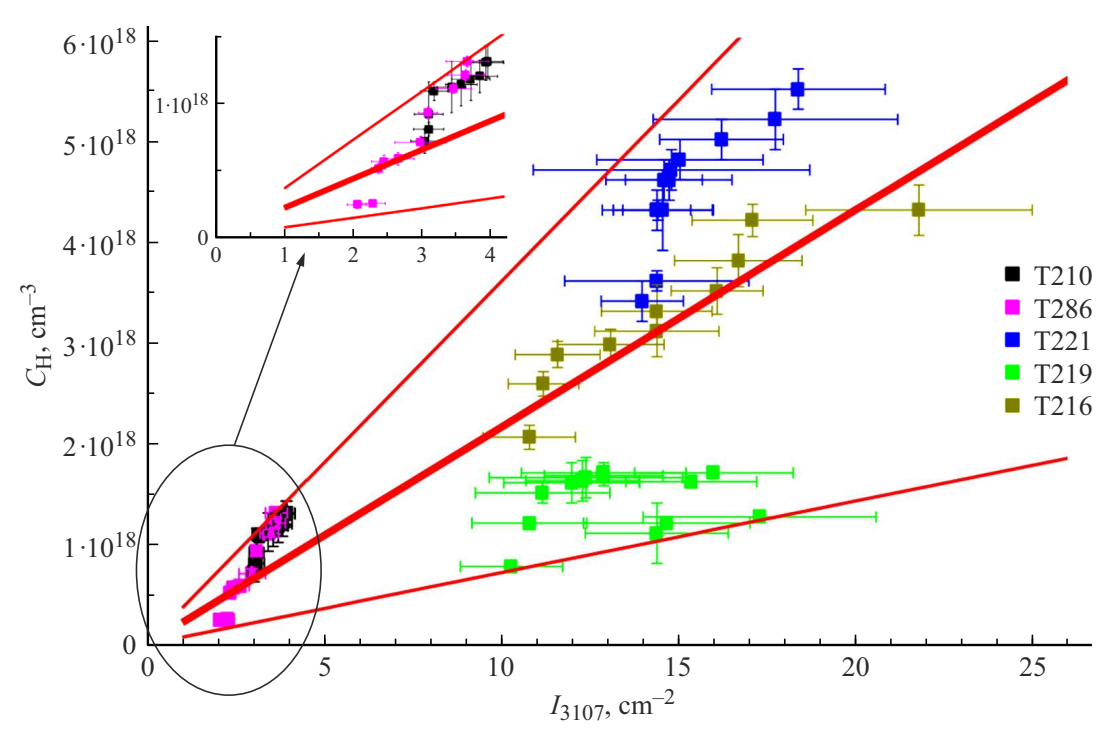


Figure 5. The ratio of IR absorption of LCM 3107 cm⁻¹ and the hydrogen concentration determined by the SIMS method for five samples marked with different colors. The linear approximation and its error limits are shown by red lines.

Results and discussion

For the five studied samples, Fig. 5 shows the results of measuring the IR absorption of LCM 3107 cm⁻¹ at the locations where the SIMS analyses were performed in comparison with the hydrogen concentrations determined by the SIMS method.

As can be seen, there is a dependence between the IR absorption of LCM 3107 cm⁻¹ and the hydrogen concentration determined by the SIMS method. We believe that the main reason for the noticeable scatter in the data is the inconsistency of the experimental methods described above — the IR absorption was measured in transmission, through the entire thickness of the sample, while the SIMS measurements affect only the surface layer. This dependence can be approximated by the ratio

$$C_{\rm H} = S_{\rm N3VH}^* \times I_{3107},$$

where $S_{\text{N3VH}}^* = (2.15 \pm 1.44) \cdot 10^{17} \text{ cm}^{-1} = (1.2 \pm 0.8) \text{ ppm cm}^{-1}$. It would be convenient to use this correlation as a normalization for determining the defect concentration N₃VH from IR spectroscopy data in LCM 3107 cm⁻¹. However, the value $S_{\rm N3VH}^*=(2.15\pm0.65)\cdot10^{17}\,{\rm cm}^{-1}$ differs greatly from the normalization obtained $S_{\rm N3VH} = (1.94 \pm 0.18) \cdot 10^{16} \, {\rm cm}^{-1}$. in the work. [19] he hydrogen concentration in diamond plates was measured by the nuclear-physical method of proton-proton collisions. The value $S_{
m N3VH}^* = (2.3 \pm 0.15) \, {
m ppm \, cm^{-1}} = (3.9 \pm 0.26) \cdot 10^{17} \, {
m cm^{-1}}$

was obtained on five samples (one questionable sample with inclusions was excluded from consideration). In [33] the value $S_{\rm N3VH}^* = (0.68 \pm 0.11) \cdot 10^{17} \, {\rm cm}^{-1} {\rm was}$ obtained on four samples (one measurement per sample) out of five (one sample strongly deviates from the correlation). Such a large scatter of data in different studies again raises the question of the forms of hydrogen incorporation into diamond that are not manifested in EPR and optical methods of analysis, including IR spectroscopy [37]. In [38] it is shown that hydrogen implanted in a high dose (a layer 1.8 µm thick with an implanted hydrogen concentration of $1.6 \cdot 10^{21} \,\mathrm{cm}^{-3}$) in diamond is also in an optically inactive state up to an annealing temperature of 1400 °C — it either does not react to IR radiation at all or absorbs very weakly. Nevertheless, hydrogen is present in diamond, because after annealing at a temperature above 1400 °C most of it collects into macroscopic blisters.

Several variants of hydrogen atom arrangement in diamond crystal lattice have been theoretically considered and calculated [23], however, IR radiation absorption should be observed in almost any variant due to the presence of a dipole moment. To date, only one variant of hidden hydrogen impurity form has been proposed — pseudomolecule H₂* [42], in which two hydrogen atoms are in neighboring interstitial positions and form a non-polar chemical bond with very low IR radiation absorption. Similar pseudomolecules H₂* have been found in silicon [43]. In combination with the absence of electrical activity and low mobility, this defect can be an electrically,

magnetically and optically inactive hydrogen reservoir in diamond.

Conclusion

Two methods of experimental study of hydrogen and N_3VH defects in natural diamonds — SIMS and IR absorption measurement have been applied. The SIMS tests were performed in crystal regions with the most uniform I_{3107} value distribution. The method of accounting for the contribution of adsorbed hydrogen to the SIMS signal was applied. The total hydrogen profiles by the depth of analysis were also presented. Theoretical calculations suggest several options for the location of hydrogen atoms in the diamond crystal structure, but most of them should lead to noticeable IR absorption, which is inconsistent with experimental observations and is not detected by standard analysis methods.

A literature analysis showed that in addition to the known forms of hydrogen in diamond, there may be other, more, hidden" configurations that are not revealed by standard analysis methods. Further research in this direction may shed light on the nature of these forms and their influence on the properties of diamond. To solve the mystery of "hidden" hydrogen in diamond, it may be necessary to use the NMR method.

Acknowledgments

The studies by the SIMS method were carried out using the secondary ion microprobe IMS7f (CAMECA, France) of the Center of Multi-User Equipment "Materials Science and Diagnostics for Advanced Technologies" (parent facility — Ioffe Institute).

Funding

The study was carried out as part of the state assignment of the Vernadsky Institute of Geochemistry and Analytical Chemistry of the Russian Academy of Sciences (GEOKHI RAS), the Institute of Geology of Ore Deposits, Petrography, Mineralogy and Geochemistry of the Russian Academy of Sciences (IGEM RAS), and with the financial support of the Russian Science Foundation as part of scientific projects № 24-22-00385 and 23-22-00453.

S.N. Shilobreeva carried out the study as part of the state assignment of GEOKHI RAS. R.A. Khmelnitsky. performed the study as part of the project 23-22-00453) (https://rscf.ru/en/project/23-22-00453/) of the Russian Science Foundation. The work of V.Yu. Prokofiev was carried out under the State assignment of IGEM RAS. S.A. Tarelkin performed the work with the financial support of the Russian Science Foundation as part of scientific project № 24-22-00385. B.Ya. Ber, D.Yu. Kazantsev and M.V. Tokarev performed the work as part of the state assignment of the A.F. Ioffe Physical-Technical Institute.

Conflict of interest

The authors declare that they have no conflict of interest.

References

- [1] P.R.W. Hudson, I.S.T. Tsong. J. Mater. Sci., 12, 2389 (1977).DOI: 10.1007/BF00553924
- [2] B. Rondeau, E. Fritsch, M. Guiraud, J.-P. Chalain, F. Notari. Diam. Relat. Mater., 13, 1658, (2004). DOI: 10.1016/j.diamond.2004.02.002
- [3] C.H. van der Bogert, C.P. Smith, T. Hainschwang, S.F. Mc-Clure. GemsGemol., 45 (1), 20 (2009). DOI: 10.5741/GEMS.45.1.20
- [4] W. Huang, P. Ni, T. Shui, G. Shi, G. Luth. GemsGemol., 55, 398 (2019). DOI: 10.5741/GEMS.55.3.398
- [5] T. Stachel, R.W. Luth. Lithos, 220 (2015).DOI: 10.1016/j.lithos.2015.01.028
- [6] C.E. Melton, A.A. Giardini. Am. Miner., 59, 775 (1974).
- [7] E.M. Smith In: Fluid and Melt Inclusions: Applications to Geologic Processes, ed. by P. LecumberriSanchez, M. Steele-MacInnis, D. Kontak (Mineralogical Association of Canada, 2020). V. 49. P. 1. DOI: .10.3749/9780921294719.ch05
- [8] E.M. Smith, M.Y. Krebs, P.-T. Genzel, F.E. Brenker. Rev. Miner. Geochem., 88, 451 (2022).DOI: 10.2138/rmg.2022.88.08
- [9] J.P.E. Sellschop, S.H. Connell, C.C.P. Madiba, E. Sideras-Haddad, M.C. Stemmet, K. Bharuth-Ram, H. Appel, W. Kundig, B. Patterson, E. Holzschuh. Nucl. Instrum. Meth. Phys. Res., 68, 133 (1992).
 DOI: 10.1016/0168-583X(92)96064-6
- [10] B.I. Green, A.T. Collins, C.M. Breeding. Rev. Miner. Geochem., **88**, 637 (2022). DOI: 10.2138/rmg.2022.88.12
- [11] A.A. Shiryaev, D. Grambole, A. Rivera, F. Herrmann. Diam.
 Relat. Mater., 16, 1479 (2007).
 DOI: 10.1016/j.diamond.2006.12.005
- [12] C. Haug, H. Gartner, J. Portmann, R. Samlenski, C. Wild, R. Brenn. Diam. Relat. Mater., 10, 411 (2001). DOI: 10.1016/S0925-9635(00)00372-1
- [13] M.I. Heggie, S. Jenkins, C.P. Ewels, P. Jemmer, R. Jones, P.R. Briddon. J. Phys.: Condens. Mater., 12, 10263 (2000). DOI: org/10.1088/0953-8984/12/49/327
- [14] M.C. Day, M.C. Jollands, D. Novella, F. Nestola, R. Dovesi, M.G. Pamato. Diam. Relat. Mater., 143, 110866 (2024). DOI: 10.1016/j.diamond.2024.110866
- [15] G. Woods, A.T. Collins. J. Phys. Chem. Solids, 44, 471 (1983).DOI: 10.1016/0022-3697(83)90078-1
- [16] W.A. Runciman, T. Carter. Solid State Commun., 9, 315 (1971). DOI: 10.1016/00381098(71)90001-9
- [17] E. Fritsch, T. Hainschwang, L. Massi, B. Rondeau. New Diam. Front. Carbon Technol., 17, 63 (2007).
- [18] F. Fuchs, C. Wild, K. Schwarz, W. Muller-Sebert, P. Koidl. Appl. Phys. Lett., 66 (2), 177 (1995). DOI: 10.1063/1.113126
- [19] J.O. Wood. An Elusive Impurity: Studying Hydrogen in Natural Diamonds. Thesis. (The University of Bristol, 2020).
- [20] M.N.R. Ashfold, L.P. Goss, B.L. Green, P.W. May, M.E. Newton, C.V. Peaker. Chem. Rev., 12, 1010 (2020).
- [21] In: Impurities and defects in group IV elements, IV–IV and III–V compounds. Part a: Group IV elements. Ed. by O. Madelung, U. Rössler, M. Schulz (Landolt-Börnstein Group III Cond. Matt. book series, 2002). V. 41A2a. P. 211.

- [22] S. Liggins. Identication of point defects in treated single crystal diamond. PhD thesis (The University of Warwick, 2010).
- [23] J.P. Goss. J. Phys.: Condens. Matter, 15, R551 (2003). DOI: 10.1088/0953-8984/15/17/201
- [24] J.P. Goss, P.R. Briddon, V. Hill, R. Jones, M.J. Rayson. J. Phys.: Condens. Matter, 26, 145801 (2014). DOI: 10.1088/0953-8984/26/14/145801
- [25] I. Kiflawi, D. Fisher, H. Kanda. Diam. Relat. Mater. 5, 1516–1518 (1996). DOI: 10.1016/S09259635(96)00568-7
- [26] C. Haug, H. Gartner, J. Portmann, R. Samlenski, C. Wild, R. Brenn. Diam. Relat. Mater., 10, 411 (2001). DOI: 10.1016/S0925-9635(00)00372-1
- [27] C.B. Hartland. A Study of Point Defects in CVD Diamond Using Electron Paramagnetic Resonance and Optical Spectroscopy. Thesis (The University of Warwick, 2014).
- [28] C. Glover, M.E. Newton, P.M. Martineau, S. Quinn,
 D.J. Twitchen. Phys. Rev. Lett., 90, 185507 (2003).
 DOI: 10.1103/PhysRevLett.90.185507
- [29] B.L. Cann. Magnetic resonance studies of point defects in diamond. Thesis (University of Warwick, 2009).
- [30] D.J.L. Coxon, M. Staniforth, B.G.E. Greenough, J.P. Goss, M. Monti, J.L. Hughes, V.G. Stavros, M.E. Newton. J. Phys. Chem. Lett., 11, 6677 (2020). DOI: 10.1021/acs.jpclett.0c01806
- [31] D.J.L. Coxon. A study of the relaxation dynamics of local vibrational modes associated with hydrogen in diamond. Thesis (University of Warwick, 2022).
- [32] F.V. Kaminsky, S.N. Shilobreeva, B.Ya. Ber, D.Yu. Kazantsev. Doklady RAN. Nauki o Zemle 494 (1), 43 (2020) (in Russian). DOI: 10.31857/S2686739720090091
- [33] F.V. Kaminsky, V.B. Polyakov, B.Ya. Ber, D.Yu. Kazantsev, G.K. Khachatryan, S.N. Shilobreeva. Chem. Geol., **661**, 122185 (2024). DOI: 10.1016/j.chemgeo.2024.122185
- [34] F. De Weerdt, A.T. Collins. Diam. Relat. Mater., **15**, 593 (2006). DOI: 10.1016/j.diamond.2006.01.005
- [35] V.T. Cherepin. *Ionnyj mikrozondovyj analiz* (Naukova Dumka, Kyiv, 1992).
- [36] D. Howell, C.J. O'Neill, K.J. Grant, W.L. Griffin, N.J. Pearson, S.Y. O'Reilly. Diam. Relat. Mater., 29, 29 (2012). DOI: 10.1016/j.diamond.2012.06.003
- [37] C. Saguy, C. Cytermann, B. Fizgeer, V. Richter, Y. Avigal, N. Moriya, R. Kalish, B. Mathieu, A. Deneuville. Diam. Relat. Mater., 12, 623 (2003). DOI: 10.1016/S0925-9635(02)00403-X
- [38] R.A. Khmelnitskiy, E.A. Zavedeev, A.V. Khomich, A.V. Gooskov, A.A. Gippius. Vacuum, 78, 273 (2005). DOI: 10.1016/j.vacuum.2005.01.038
- [39] F.A. Stevie. Secondary Ion Mass Spectrometry. Applications for Depth Profiling and Surface Characterization (Momentum Press, N. Y., 2016).
- [40] R.G. Wilson, F.A. Stevie, C.W. Magee. Secondary Ion Mass Spectrometry: A Practical Handbook for Depth Profiling and Bulk Impurity Analysis (Wiley, N.Y., 1989).
- [41] International Standard ISO 18114:2003(E). Surface Chemical Analysis Secondary-Ion Mass Spectrometry Determination of Relative Sensitivity Factors from Ion Implanted Reference Materials (2003).
- [42] J.P. Goss, R. Jones, M.I. Heggie, C.P. Ewels, P.R. Briddon,
 S. Oberg. Phys. Rev. B, 65, 115207 (2002).
 DOI: 10.1103/PhysRevB.65.115207

[43] E.E. Chen, M. Stavola, W.B. Fowler, J.A. Zhou. Phys. Rev. Lett., 88, 245503 (2002). DOI: 10.1557/PROC-813-H6.1

Translated by J.Savelyeva